



**University of Dundee**

**Origin and age of The Hillocks and implications for postglacial landscape development in the upper Lake Wakatipu catchment, New Zealand**

McColl, Samuel T.; Cook, Simon J.; Stahl, Timothy; Davies, Timothy R. H.

*Published in:*  
Journal of Quaternary Science

*DOI:*  
[10.1002/jqs.3168](https://doi.org/10.1002/jqs.3168)

*Publication date:*  
2019

*Document Version*  
Peer reviewed version

[Link to publication in Discovery Research Portal](#)

*Citation for published version (APA):*  
McColl, S. T., Cook, S. J., Stahl, T., & Davies, T. R. H. (2019). Origin and age of The Hillocks and implications for postglacial landscape development in the upper Lake Wakatipu catchment, New Zealand. *Journal of Quaternary Science*, 34(8), 685-696. <https://doi.org/10.1002/jqs.3168>

**General rights**

Copyright and moral rights for the publications made accessible in Discovery Research Portal are retained by the authors and/or other copyright owners and it is a condition of accessing publications that users recognise and abide by the legal requirements associated with these rights.

- Users may download and print one copy of any publication from Discovery Research Portal for the purpose of private study or research.
- You may not further distribute the material or use it for any profit-making activity or commercial gain.
- You may freely distribute the URL identifying the publication in the public portal.

**Take down policy**

If you believe that this document breaches copyright please contact us providing details, and we will remove access to the work immediately and investigate your claim.

1 **Research paper**

2

3 **Title:** Origin and age of The Hillocks and implications for post-glacial  
4 landscape development in the upper Lake Wakatipu catchment, New Zealand.

5

6 **Running Title:** Origin of The Hillocks

7

8 Samuel T. McColl\*<sup>1</sup>. Simon J. Cook<sup>2</sup>. Timothy Stahl<sup>3</sup>. Timothy R. H. Davies<sup>3</sup>.

9 <sup>1</sup>Geosciences Group, School of Agriculture and Environment, Massey

10 University, New Zealand. \* Corresponding Author: [s.t.mccoll@massey.ac.nz](mailto:s.t.mccoll@massey.ac.nz)

11 <sup>2</sup>Geography and Environmental Science, School of Social Sciences,

12 University of Dundee, UK

13 <sup>3</sup>School of Earth and Environment, University of Canterbury, New Zealand

14

15

16        **Abstract**

17        Ambiguous landscape histories can arise from equivocal or incomplete  
18        geomorphological, sedimentological or geochronological evidence. In this study,  
19        we apply quantitative analyses to robustly assess the origin and age of a field of  
20        rounded mounds, known as ‘The Hillocks’. Using clast analysis, the sediment is  
21        shown to be consistent with a landslide origin but inconsistent with other glacial  
22        sediments in the region. Cosmogenic  $^{10}\text{Be}$  exposure age dating suggests The  
23        Hillocks formed  $\sim 8$  ka. Ground-penetrating radar (GPR) reveals that the deposit  
24        rests upon deltaic foreset beds, combined with topographic data, we calculate a  
25        deposit volume of  $\sim 15\text{-}27 \text{ M m}^3$ , consistent with the estimated volume of the  
26        proposed source area. Overall, our data support a rock avalanche origin,  
27        indicating that by 8 ka the valley was ice-free at The Hillocks location, and the  
28        level of Lake Wakatipu was lower than 340 m asl by this time. The Dart River  
29        delta shoreline was situated somewhere between The Hillocks and the present-  
30        day shoreline at that time, and has prograded at a maximum average rate of 1 m  
31         $\text{a}^{-1}$  since  $\sim 8$  ka. These findings are significant given the lack of landforms by  
32        which to constrain glacial or post-glacial landscape histories in this region of New  
33        Zealand.

34

35        **Keywords**

36        Rock avalanche, landform origin, kame, paraglacial, Lake Wakatipu

37

## 38 **Introduction**

39       Glacial chronologies, landscape histories, and hazard assessments must be  
40 underpinned by reliable assessment of landform origin. Glacial landforms, such  
41 as moraines, can be geomorphologically and sedimentologically similar to  
42 landforms produced by other processes such as landslides (e.g. Hewitt, 1999,  
43 2009; Putnam et al. 2010a; Ostermann et al. 2012, Cook et al., 2013, Schleier et  
44 al., 2015), leading to possible misidentification. In New Zealand, debates over  
45 landform origin bear on broader debates about the extent to which the climates  
46 and glacier fluctuations of the Northern and Southern Hemispheres are  
47 connected (e.g. Denton et al., 1999; Schaefer et al., 2006; Schaefer et al., 2009;  
48 Winkler 2014). New Zealand glaciations are important in this context because  
49 New Zealand is one of the few landmasses within the Southern Hemisphere  
50 where a terrestrial record of glaciation is preserved (Alloway et al., 2007;  
51 Sutherland et al., 2007). However, New Zealand is also prone to slope instability  
52 as a consequence of high relief, strong seismic activity, high precipitation, and  
53 deglaciation, meaning that the Quaternary landform record comprises a complex  
54 mix of mass movement and glacial deposits (e.g. Alexander et al. 2014;  
55 Reznichenko et al. 2016). Additionally, high rates of fluvial erosion and  
56 aggradation can rapidly modify and obscure these deposits. Differentiating  
57 between these landforms is essential if researchers are to make reliable  
58 paleoenvironmental and landslide hazard assessments; robust age assessment  
59 and quantitative analyses of landform characteristics provide a means for reliable  
60 landform identification and consequent landscape interpretations.

61 In this study, we extend earlier work by McColl and Davies (2011) who  
62 investigated 'The Hillocks' in Otago, New Zealand (Figure 1), and argued it was  
63 produced by a rock avalanche. The Hillocks landform comprises an array of  
64 mounds that rise above the surrounding Dart River floodplain. It had formerly  
65 been assumed to be a glacial kame deposit (Kenny and Hayward, 1993), and  
66 has been used in glacial reconstructions for this region (Barrell, 2011). McColl  
67 and Davies' (2011) argument for a rock avalanche origin was based on the  
68 qualitative similarity of the deposit morphology and sedimentology to other rock  
69 avalanche deposits. Here, we apply a quantitative assessment of morphology,  
70 material properties and subsurface investigation to provide a more robust means  
71 of assessing the landform origin. In addition, we apply cosmogenic  $^{10}\text{Be}$  surface  
72 exposure dating to assess whether or not the landform age is consistent with a  
73 Late Glacial origin as previously assumed. The findings presented here shed  
74 new light on the post-glacial landscape evolution in this part of New Zealand.

75

76

## 77 **Regional setting and site description**

78 The Hillocks is an array of rounded to irregular-shaped mounds, up to 20 m in  
79 height and 140 m in long-axis, that are situated on the floodplain of the Dart River  
80 and below the south western flank of Mount Alfred, Otago, New Zealand (Figure  
81 1). The Dart River is a large, braided river that, along with the neighbouring Rees  
82 River, feeds into the Dart-Rees delta at the head of Lake Wakatipu at ~309 m

83 above sea level (Figure 1). The Dart River and its tributaries drain a mountainous  
84 section of the south-eastern Southern Alps, which has peaks in excess of 2500  
85 m above sea level. The basement geology is the Mesozoic Haast Schist Group  
86 (Turnbull, 2000), with melange and slightly foliated volcanoclastic Caples terrane  
87 predominant in the Humboldt Mountains to the west, and higher-grade schists  
88 (textural zone IIB and IV with well-developed foliation and alteration) of the  
89 Caples and Rakaia terranes in the Barrier Range and Forbes Mountains to the  
90 north and east (Figure 1). Immediately adjacent to The Hillocks, on the western  
91 rock slope of the Dart Valley, the (textural zone IIB) semischist is replaced by the  
92 Bold Peak Formation, a dominantly-sandstone member of the Caples Terrane  
93 with textural zone IIA giving way to textural zone I (i.e. unmetamorphosed)  
94 towards the top of the rock slope (Figure 1; Turnbull, 2000). The source area for  
95 The Hillocks rock avalanche, proposed by McColl and Davies (2011) is within the  
96 Bold Peak Formation (Figure 1) at the top of the rock slope. The north-striking  
97 West Wakatipu Fault, which is likely active (Barrell, 2019), separates the Bold  
98 Peak Formation from the IIB semischist, and traverses the slope below the  
99 proposed rock avalanche source area. The potential for seismically-triggered  
100 slope failures in the region is high, with the active Alpine Fault and Nevis-  
101 Cardrona Fault, and numerous potentially active faults (including the West  
102 Wakatipu Fault) located within 60 km of The Hillocks. Stirling et al. (2012)  
103 estimate a regional probabilistic peak ground acceleration of 0.5-0.6 g over a  
104 475-year return time, resulting in a high probability of co-seismic slope failures in

105 this region. At least one of the large landslides in the Dart River catchment is  
106 thought to have been co-seismically generated (Wood et al., 2011).

107 [Insert Figure 1]

108 The basin of Lake Wakatipu and the catchments that feed into it have been  
109 glaciated during the Quaternary (Turnbull, 2000; Barrell, 2011). Today, the ~6 km  
110 long Dart Glacier sits at the head of the Dart catchment, but it once would have  
111 fed a much larger glacier system that filled the Wakatipu basin during Quaternary  
112 glaciations. Lake Wakatipu, 309 m above sea level, now occupies this glacially  
113 overdeepened trough, which is ~80 km long, with a maximum depth (to lake-bed,  
114 rather than bedrock trough) of 380 m (Brodie and Irwin, 1970). At its maximum  
115 extent during the Otira Glaciation (marine isotope stages [MIS] 2-4; ~65 ka to  
116 11.5 ka; Barrell, 2011), the glacier would have terminated at the southern end of  
117 the lake (Figure 1 C), where it deposited a suite of large terminal moraines  
118 (Barrell, 2011). These moraines are some 86 km down-valley from The Hillocks  
119 and 135 km down-valley from the present-day Dart Glacier terminus. Glacial  
120 erosional evidence and scattered glacial deposits exist high on the valley sides  
121 throughout the Wakatipu basin and, along with the Otiran terminal moraine, has  
122 allowed mapping of the maximum extent of glaciations (Barrell, 2011). However,  
123 there is sparse evidence for reconstructing the post-LGM deglaciation history of  
124 the Wakatipu basin, by contrast with other regions of New Zealand where late-  
125 Glacial and Holocene terminal positions have been identified (e.g. by moraines  
126 associated with the Antarctic Cold Reversal) (e.g. Putnam et al., 2010b).

127        There is evidence, represented by stranded lake shorelines, alluvial fan  
128 terracing, and delta foresets, that Lake Wakatipu has previously been up to ~50  
129 m higher than the present day (Kober, 1999). Radiocarbon dating of wood  
130 excavated from one of the shorelines cut 26 m above the current lake level,  
131 suggests the lake was at that level at ~10 ka BP (Bell, 1992). The highest  
132 preserved shoreline (~ 50 m above modern lake level, at ~360 m asl), is  
133 suggested to have formed at least 1000 years earlier (Bell, 1992, Kober, 1999;  
134 Thomson, 1996; Sutherland et al., 2019). Other than this, little is known of the  
135 absolute timing of prehistorical lake level changes or positions of the Dart River  
136 delta. Foreset beds associated with a Lake Wakatipu delta are preserved east of  
137 Mt Alfred at an elevation of ~358 m asl (Kober, 1999), which is about 10 m above  
138 the modern Dart River floodplain at The Hillocks.

139

## 140        **Methods**

141        To assess the origin, history, and characteristics of The Hillocks, we use a  
142 combination of morphological, sedimentological, geophysical, and chronological  
143 tools.

### 144        *Lithology and sedimentology*

145        Samples of 50 clasts were extracted from river-cut exposures of The Hillocks  
146 sediment as well as from a range of other sediment types for use as  
147 comparisons. All clast measurements were made by a single person for  
148 methodological consistency. Comparison sites included river gravels from the



149 neighbouring Rees River (hereafter referred to as 'river sediment'), diamictites of  
150 glacial origin either from till exposures cut by the Rees River, or from glacial  
151 deposits reworked by debris flows at Muddy Creek (as reported in Cook et al.,  
152 2014; hereafter referred to as 'glacial sediment'), and from alluvial fan deposits  
153 close to Kinloch, ~8 km south of The Hillocks (hereafter referred to as 'alluvial fan  
154 sediment'). Following the methodology of Benn (2004), the long (a), intermediate  
155 (b) and short (c) axes of each clast were measured, as well as the roundness  
156 according to the classification scheme of Powers (1953), and facets, which would  
157 be expected in samples influenced by subglacial wear.  $C_{40}$  values (i.e. the  
158 proportion of clasts with a c:a axial ratio of  $\leq 0.4$ , which represent more slabby  
159 and elongate shapes) were calculated for each sample, as well as the RA  
160 (relative angularity) value (i.e. the proportion of clasts in each sample that were  
161 classed as angular or very angular). Plots of  $C_{40}$  against RA have been shown to  
162 be useful in differentiating between samples of different origins, including  
163 between glacial and rock avalanche deposits (e.g. Benn and Ballantyne, 1994;  
164 Benn, 2004; Cook et al., 2013).

165

#### 166 *Age assessment*

167 To assess the age of The Hillocks, we applied in-situ cosmogenic  $^{10}\text{Be}$   
168 exposure dating to boulders on mounds and other deposits assumed to be  
169 related to The Hillocks. One boulder (WP166) was sampled from a boulder  
170 accumulation below the rock avalanche source area suggested by McColl and

171 Davies (2011), one boulder (HB24) was sampled from the debris fan at the base  
172 of the hillslope, and two boulders (HB14 & HB20) were sampled from mounds on  
173 the valley floor (Figure 2). All samples appeared to be of similar lithology –  
174 slightly weathered, slightly foliated grey sandstone, with thin dark veins or  
175 laminations, and mm-cm thick quartz veining common, and are inferred to be part  
176 of the Bold Peak Formation. To minimise the chance of selecting boulders or  
177 boulder surfaces that would provide unrepresentative exposure ages, we applied  
178 the following sampling criteria: i) the boulders were larger than 1 m in diameter;  
179 ii) the boulders were at the higher parts of the local topography (i.e. on top of  
180 mound, fan, boulder pile) and therefore less likely to have rolled/toppled since  
181 their original emplacement; iii) the sampled surface of the boulder was more than  
182 0.5 m above any surrounding soil; and iv) for the debris fan and floodplain, the  
183 boulders had mean Schmidt hammer (N-type) rebound values that were within  
184 the standard deviation range of all sampled boulders – rebound values were not  
185 collected from boulders near the hypothesised source area. Schmidt hammer  
186 rebound values (c.f. Goudie, 2006) were measured at least three times for each  
187 boulder, discarding the lowest measurement on each boulder. Additionally,  
188 rebound values were measured on several boulders in the Dart River to compare  
189 fresh (fluvially eroded) boulders with the weathered boulders sampled for  
190 cosmogenic dating.

191 Where possible, surfaces with visible, protruding quartz veins were targeted  
192 for cosmogenic sampling. A hammer and chisel were used to chip off 1-3 cm  
193 (average of 1.5 cm) thickness of rock and quartz veins from the boulder surfaces.

194 Topographic shielding corrections were calculated from skyline surveys at each  
195 sampling site, and boulder position and elevation measured with a Trimble  
196 GeoXH differential GPS, corrected against the Land Information New Zealand  
197 geodetic network.

198 Quartz was isolated following standard mineral separation procedures.  
199 Beryllium targets for two of the samples (HB20 and WP166) were prepared at  
200 University of Canterbury and, the other two (HB14 and HB24) were prepared at  
201 GNS Science and Victoria University of Wellington. The beryllium of samples and  
202 blanks was measured by the GNS Science Accelerator Mass Spectrometer. For  
203 WP166 and HB20 correction was made for a single processing blank (NZ0724)  
204 ( $5.5 \pm 1.7 \cdot 10^7$  a  $^{10}\text{Be}$ ; < 7%) and for HB14 and HB24 two processing blanks  
205 (KV322 and KV332) were averaged and the correction was less than 12 % ( $1.8 \pm$   
206  $0.3 \cdot 10^5$  a  $^{10}\text{Be}$ ). Exposure ages, using processing-blank corrected data, were  
207 calculated using the online exposure age calculator (version 3; Balco et al., 2008)  
208 using the Putnam et al. (2010a) Macaulay valley, New Zealand  $^{10}\text{Be}$  production  
209 rate, and the time-dependent 'LSDn' scaling method.  $^{10}\text{Be}$  ages presented in this  
210 study are not corrected for erosion; though up to ~ 1 cm of quartz vein relief on  
211 the boulders indicates that at least some surface erosion has taken place since  
212 exposure. The ages are also not corrected for snow shielding or burial by loess  
213 or soil but these potential influences were minimised by selecting protruding  
214 boulders from local topographic highs.

215 [Insert Figure 2 here]

216        *Sub-surface investigation*

217        Ground Penetrating Radar (GPR) was used to assess the internal structure  
218 and depth (i.e. total thickness) of the sediments comprising the mounds, and the  
219 nature of underlying and overlying sediments. A PULSE EKKO PRO GPR was  
220 deployed across four transects (Figure 2) toward the distal edge of the mound  
221 distribution; Transect A is 100 m long, parallel to the Dart Valley axis, and  
222 extends over a mound at the downstream end; Transect B is 100 m long,  
223 oriented perpendicular to the valley axis and crosses two mounds of low (< 5 m)  
224 relief; Transect C is 200 m long, oriented perpendicular to the valley axis, and  
225 crosses one small (< 2 m high) mound; Transect D is 150 m long, parallel to the  
226 valley axis, and crosses two mounds. For transects A, B and D, 100 MHz  
227 unshielded antennas were used; 50 MHz antennas were used for Transect C.  
228 Topographic profiles were measured using tape and laser rangefinder (Transect  
229 B) and differentially-corrected Trimble GPS (Transects A, C, and D). Radargrams  
230 were prepared using EKKO Project 3 software. An average velocity of 0.08 m/ns,  
231 as assessed by three common mid-point surveys and hyperbola velocity  
232 calibration, were applied to all radargram transects to apply topographic and  
233 depth corrections. Dewow and AGC gains were applied to enhance deeper  
234 reflectors.

235

236        *Deposit volume and morphometry*

237 The size distribution and volume of mounds comprising The Hillocks were  
238 measured to characterise the geometry of the deposit and provide a revised  
239 minimum estimate for the landform's total volume. An aerial LiDAR point cloud  
240 (of classified ground points) of the Dart River floodplain for The Hillocks area was  
241 collected and supplied by Otago Regional Council in 2019. This was converted to  
242 a 1 m resolution digital elevation model (DEM) and hillshade model. Outlines of  
243 the mounds were mapped from the hillshade model and accompanying LiDAR  
244 orthophotos. Mounds were mapped only if there was high confidence in the  
245 presence of a mound; about two-thirds of the mapped mounds were verified in  
246 the field. The deposit is partly covered by loess and alluvium, the latter indicated  
247 by the presence of paleo braid channels between mounds and fluvially-rounded  
248 gravels overlaying the angular diamicton exposed in bank sections (McColl and  
249 Davies, 2011). The depth of the alluvium ( $z$ ) was estimated by ground  
250 penetrating radar (GPR). To account for this alluvial cover in measuring mound  
251 geometry, we widened the extent of the mound polygons by a constant buffer  
252 distance ( $w$ ), assessed by  $w = \tan\beta \cdot z$ , where  $\beta$  is the angle of the sides of the  
253 mounds (Figure 2). A representative slope angle for all mounds was estimated by  
254 calculating the mean pixel value of a 1 m resolution slope raster set within a 5 m  
255 buffer (5-10 m inside from the mapped mound extent) of mounds of greater than  
256  $150 \text{ m}^2$  (Figure 2).

257 A minimum (but maximum empirically-constrainable) volume of subaerial  
258 mounds was calculated by multiplying the mound area by average mound height.  
259 The buried volume of mounds beneath the alluvial cover was added to this

260 volume calculation by multiplying the mound area by the thickness of alluvial  
261 cover (z), with the mound area extended by (half of) the buffer width (w) to  
262 account (the wedge-shaped) volume of outer mound buried by alluvium. In  
263 calculating mound volume, we ignore any mounds removed by erosion or buried  
264 by fluvial or aeolian sediments, but consider that post-event changes in deposit  
265 morphology are unlikely to affect our volume estimate by more than  $\pm 10\%$ . We  
266 plotted the size frequency distribution of the mounds (volume and area). Cross-  
267 sections were also constructed to show the gross topographic profile of the  
268 mounds at directions perpendicular and parallel to the assumed rock avalanche  
269 travel direction across the valley, using a swath of random elevation points on the  
270 mounds. The remaining volume of the rock avalanche beneath the rock  
271 avalanche mounds is calculated by assessing the inferred planimetric area of the  
272 entire deposit, and multiplying by a thickness (i.e. depth to the base of the rock  
273 avalanche deposit) measured by GPR. The planimetric area was inferred to  
274 extend 50-100 m beyond the visible extent of the mounds, based on  
275 interpretation of the radargrams.

276

## 277 **Results**

### 278 *Sedimentology*

279 The Hillocks sediments are angular to very angular, clast-supported, poorly  
280 sorted, and lack bedding structures (Figure 3). The majority of the sediments are  
281 the same rock type, slightly metamorphosed sandstone similar to that found in

282 the proposed source area and assumed to be Bold Peak Formation. Along the  
283 northern edge of the mapped deposit, pelitic semischist clasts were present,  
284 which are similar to pelitic semischist found in-situ on the lower western slopes  
285 adjacent to The Hillocks, and inferred to be part of the IIB semischists mapped by  
286 Turnbull (2000) (Figure 1). The Hillocks sediments represent a distinct  
287 population in terms of clast shape and roundness when compared to other  
288 sediment types found in the local area (Figure 4). Whilst the range of  $C_{40}$  values  
289 of The Hillocks sediment are not dissimilar to glacial, fluvial and alluvial fan  
290 sediments, the overall average  $C_{40}$  value (60 %) is lower than other sediments in  
291 the region, and the RA value is much higher (82 % on average). The  $C_{40}$  and RA  
292 values are compatible with  $C_{40}$  and RA values measured for rockfall and other  
293 supraglacial debris found in New Zealand and globally (Figure 4); we note a  
294 difference in  $C_{40}$  values for the fluvial and glacial sediments in the Wakatipu  
295 region compared to other localities, which may relate to a difference in lithology.  
296 Facets were not found on any of The Hillocks clasts, whereas they were  
297 relatively common in the glacial (mean =  $47 \pm 8$  %; from 6 sample sets), fluvial  
298 (mean =  $24 \pm 12$  %; from 3 sample sets), and alluvial fan (mean =  $86 \pm 3$  %; from  
299 2 sample sets) facies in the region.

300 [Insert Figure 3 here]

301 [Insert Figure 4 here]

302 *Age assessment*

303 The boulders selected for  $^{10}\text{Be}$  cosmogenic measurement yielded mean  
304 Schmidt hammer (SH) rebound values within the standard deviation of the SH-  
305 measured boulders from the mounds and debris fan samples (Figure 5). This  
306 provided further support, to the geomorphic criteria for sample selection, that the  
307  $^{10}\text{Be}$  sampled boulders were representative of The Hillocks mounds; that is to  
308 say it is unlikely that they have anomalously young (e.g. from overturning or  
309 burial) or old (e.g. from inheritance) exposure ages. The boulders in the active  
310 river channel, which are fluvially-abraded, had a significantly higher mean  
311 rebound value ( $\bar{x}$  56.5,  $\sigma$ 4.4;  $T = 4.95$ ;  $df = 9$ ,  $p = 0.000$ ; for a two sample,  
312 unequal variances, one-tail t-test) than on the mounds or debris fan, as expected.  
313 The mean SH value ( $\bar{x}$  44,  $\sigma$ 5.3) for all measured mound boulders was slightly  
314 lower than the mean value ( $\bar{x}$  45.6,  $\sigma$ 4.1) for the debris fan boulders, but not  
315 significantly higher at  $\alpha=0.05$  (for a two sample, unequal variances, one-tail t-test;  
316  $T = 1.56$ ;  $df = 15$ ;  $p = 0.07$ ).

317 The  $^{10}\text{Be}$  cosmogenic measurements yielded ages ( $\pm 1 \sigma$ ) of  $8.3 \pm 0.6$  and  $7.6$   
318  $\pm 0.5$  ka for the mound boulders,  $7.0 \pm 0.5$  ka for the debris fan boulder, and  $7.6$   
319  $\pm 0.3$  ka for the source area boulder (Table 1; Figure 5). These ages are  
320 statistically indistinguishable at 95 % confidence level, according to a reduced  
321 chi-squared test (with a weighted mean and standard deviation of  $7.6 \pm 0.4$ ;  $X_R^2 =$   
322  $1.08$ ,  $\kappa = 2.63$ ; following equations of Jones et al. 2019). This suggests that they  
323 could represent a single event. However, as the source area boulder is on a  
324 separate landform to The Hillocks mounds and debris fan (i.e. a ridge of  
325 boulders), it is more appropriate to exclude it from an age estimate for The



326 Hillocks. Based on sedimentology there is no reason to treat the debris fan as  
327 different to the mounds, and a fan is expected to have been produced at the  
328 base of the slope by the same flow of material that went on to form the mounds.  
329 Nonetheless, congruent with the SH R-values, the debris fan has a younger  $^{10}\text{Be}$   
330 exposure age than the mounds (without overlapping of  $1 \sigma$  uncertainties). The  
331 debris fan boulder is located on top of the debris fan, and while it may have  
332 originated in the same event, it is quite possible that this boulder was transported  
333 to the debris fan at a later date, some  $\sim 1$  ka after the formation of the mounds;  
334 we might expect that the fan would continue to build after its initial formation. If  
335 the debris fan boulder is excluded, the two mound boulders yield a weighted  
336 mean age and standard deviation of  $7.9 \pm 0.4$  ka (which is close to the normal  
337 kernel density, or camel diagram, estimate of 7.8 ka; Figure 5). If the debris fan  
338 sample is included it yields a weighted mean age of  $7.6 \pm 0.5$  ka.

339 [Insert Table 1 here]

340 [Insert Figure 5 here]

#### 341 *Subsurface information*

342 Radargrams for all transects reveal layers of sediment draping between the  
343 mounds, interpreted to be fluvial sediments/flood deposits associated with an  
344 abandoned braid plain (with lower boundary marked by blue line in Figure 6). The  
345 thickness of alluvium is estimated from the radargrams to be up to 4 m, but  
346 mostly around 2 m thick. A value of 2 m was used as a representative thickness  
347 (z) for calculating mound volume. Reflectors below the alluvial drape and in the

348 mounds are chaotic, with hyperbola tails likely indicating blocky or boulder  
349 structure, consistent with bouldery diamicton. The chaotic material generally  
350 overlies more structured, parallel, gently inclined reflectors interpreted to be  
351 bedded fluvial sediments (or topset beds) formed by migrating braid channels  
352 and bars, but in places the base is difficult to distinguish. The contact between  
353 the upper chaotic material and the lower structured material is more visible, and  
354 relatively planar, in the valley-parallel transects (Figure 6; red line on A and D)  
355 and the thickness of the chaotic material appears to be greater down valley (i.e.  
356 thicker in Transect D than in Transect A). The contact is more difficult to discern  
357 in the valley-perpendicular transects (Figure 6; red line on B and C), and is more  
358 undulating and possibly stepping down towards the west / valley-centreline  
359 (Figure 6; red line on C), suggesting terraces. The thickness of the chaotic  
360 material is estimated to be between 4 to 12 m. In Transects A and D, which are  
361 parallel to the valley axis, more steeply inclined, parallel reflectors (orange lines  
362 in Figure 6) dip down-valley and are interpreted as deltaic foreset beds of a  
363 prograded delta (with upper contact with topset or other alluvium represented by  
364 orange line in Figure 6).

365 [Insert Figure 6 here]

### 366 *Deposit volume and morphology*

367 The volume of material occupied by the 169 mapped mounds is calculated to  
368 be 1.6 M m<sup>3</sup>. The area of the entire mapped deposit is calculated as 2 M m<sup>2</sup>, and  
369 using the 4-12 m range of thickness estimated by GPR, suggests a further 8 to

370 24 M m<sup>3</sup> is buried beneath the floodplain alluvium, giving a total deposit volume  
371 likely between ~10 and 26 M m<sup>3</sup>. The deposit is dominated by mounds with areas  
372 between 500-2000 m<sup>2</sup> and volumes between 1000-5000 m<sup>3</sup>, with smaller mounds  
373 (according to area, volume and height; Figure 7 A, B, and D respectively)  
374 towards the east. The gross morphology of The Hillocks appears to thin outwards  
375 towards the edges in the transverse swath (Figure 7C), but with the highest  
376 mound features not at the centre of the transect due to two large mounds at 350  
377 m and 950 m from the section origin (Figure 7C). In an across-valley direction  
378 (longitudinal relative to hypothesised rock avalanche travel direction; Figure 7D),  
379 the mounds are at their highest at about 550 m from the origin, and reduce in  
380 height gradually across valley to the east, and decline more sharply towards the  
381 west (Figure 7D). The base of The Hillocks gradually rises towards the east (from  
382 about the 600 m distance mark on Figure 7D).

383 [Insert Figure 7 here]

384

## 385 **Discussion**

### 386 *Origin of The Hillocks*

387 Our results support the conclusion of earlier work by McColl and Davies  
388 (2011) who had suggested a landslide origin for The Hillocks. Sedimentological  
389 data confirm that The Hillocks debris is angular and mostly monolithic, is poorly  
390 sorted and lacks bedding structures (i.e. is a diamicton; Figure 3). These

391 characteristics are consistent with other observations of rock avalanche  
392 sedimentology (e.g. Hewitt, 1999, 2009; Dufresne et al., 2016; Cook et al., 2013;  
393 Dunning, 2006), but different from glacially derived sediments in the region  
394 (Figure 4). The morphology and presence of mounds making up The Hillocks are  
395 also consistent with rock avalanche deposits (Dufresne and Davies, 2009).  
396 McColl and Davies (2011) observed a crudely radial alignment of mounds  
397 spreading out from the western valley side. The morphometric analyses in this  
398 study (Figure 7 C & D) support this, demonstrating a lowering of mound height  
399 towards the east (i.e. distal from source) and a lowering of heights on the lateral  
400 margins of the deposit, which is consistent with a rock avalanche spreading and  
401 thinning out over a relatively unconfined surface (Dufresne, 2009; Paguican et  
402 al., 2014); we note that there may have been some terracing of the substrate  
403 representing several metres of relief across the valley floor (Figure 6C). The  
404 reduction in mound size (Figure 7 A & B) with travel distance is also common for  
405 avalanche deposits (Paguican et al., 2014), but there is no obvious reason why a  
406 glacier would create such a notable cross-valley distribution of mound sizes.  
407 Further, the geochronological data presented here indicate that The Hillocks was  
408 deposited at ~7.9 ka. An earlier compilation of mapped landforms by Barrell  
409 (2011) was used to reconstruct a series of ice limits for the Wakatipu Glacier; a  
410 Late MIS2 (18-30 ka) ice margin, incorporating The Hillocks, was drawn for the  
411 Dart valley. The cosmogenic dating presented here indicates that The Hillocks  
412 formed after the Late Glacial, and certainly after MIS2. We suggest that the  
413 glacier terminus would likely have retreated beyond The Hillocks well before 7.9

414 ka for two reasons: i) geological evidence (e.g. Kober, 1999) and topographic  
415 profiling suggest that the lake would have extended farther up valley than The  
416 Hillocks, making a stable terminal position at or downstream of The Hillocks  
417 unlikely; and ii) the Dart River must have subsequently prograded downstream of  
418 The Hillocks prior to their formation, as supported by the observation in the  
419 radargrams (Figure 6) of deltaic foreset beds underlying the diamicton. There is  
420 also no evidence (c.f. Ballantyne, 2018) of a glacial readvance over The Hillocks,  
421 which could have reset exposure ages; although it is recognised that a thin  
422 glacier over a short duration may not cause an obvious modification (Cook et al.,  
423 2013). Moreover, glacial chronologies from other eastern South Island glacial  
424 valleys (e.g. Putnam et al., 2010b; Kaplan et al., 2013) have shown that by about  
425 8 ka glacier limits were closer to their Little Ice Age and present-day limits than  
426 their late Glacial (i.e. Antarctic Cold Reversal; 14.5-12.7 ka) limits, indicating  
427 relatively small Holocene glaciers. The Hillocks is almost 50 km down valley of  
428 the present-day Dart Glacier terminus, so by 8 ka the terminus is likely to have  
429 been much farther up valley than The Hillocks. Taken together, it is difficult to  
430 reconcile the observations in this study and McColl and Davies (2011) with the  
431 long-held view that The Hillocks represent a glacial deposit (Kenny and Hayward,  
432 1993). The evidence presented in this study is consistent with a rock avalanche  
433 origin for The Hillocks.

434

435 *Rock avalanche volume and source*

436 Using GPR and new topographic data, the volume of The Hillocks deposit is  
437 estimated to be within a range of 10 to 26 M m<sup>3</sup>. To estimate the total rock  
438 avalanche deposit volume, we round these values up to 11-27 M m<sup>3</sup> to  
439 conservatively account for an unquantified amount of material deposited at the  
440 base of the source area and possibly along the transport path. This range fits  
441 with the 22.5 M m<sup>3</sup> volume estimated for the source area hypothesised by McColl  
442 and Davies (2011), who had identified a basin at the top of the western hillslope  
443 (Figure 8). The lithology of the rocks found in the source area also appears  
444 similar to the sediments in The Hillocks and debris fan. A rock type, of minor  
445 overall constituent, was found within a mound on the northern edge of The  
446 Hillocks and appears to be the same as a band of in-situ bedrock (pelitic  
447 semischist of textural zone IIB; Figure 1) observed near the base of the valley  
448 slope. This suggests there must have been at least some additional entrainment  
449 of material by the rock avalanche. Overall, we provide further support for the  
450 source area proposed by McColl and Davies (2011). While not entirely  
451 convincing in form as a landslide source area, rockfall and other erosion over the  
452 past 8 ka would have modified this basin considerably, explaining why today it  
453 poorly resembles a landslide scar.

454

455 [Insert Figure 8 here]

456 *Implications for landscape development chronology*

457 The identification of The Hillocks as a landslide deposit has implications for  
458 understanding glacial and post-glacial landscape change in the Wakatipu region.  
459 Landforms of glacial deposition are sparse in the Wakatipu region (Barrell, 2011),  
460 and very few deposits of any origin have been dated. Our results indicate that  
461 The Hillocks deposit cannot be used to directly reconstruct former glacier extent  
462 in the region, but its presence demonstrates that the glacier terminus was farther  
463 up the Dart valley by ~8 ka, and probably much closer to the present day Dart  
464 Glacier terminus, consistent with other glacial reconstructions from the eastern  
465 Southern Alps (Putnam et al., 2010b; Kaplan et al., 2013). Radiocarbon dating of  
466 wood fragments unearthed in lake sediments near Queenstown and Frankton  
467 demonstrate that Lake Wakatipu had begun forming (i.e. the glacier terminus had  
468 retreated past Queenstown) by at least ~10 ka BP (Bell, 1992). Taken together  
469 with data presented in this study, the position of the ice front can be constrained  
470 as having been north of Queenstown/Frankton by ~11 ka BP to somewhere likely  
471 well north (up valley) of The Hillocks by ~8 ka. Further geochronological data are  
472 clearly desirable to better constrain ice positions, but this is challenging given the  
473 lack of glacial deposits and other target landforms.

474 The age and position of The Hillocks also provides some constraint on the  
475 prehistoric timing and positions of the Dart River delta and the level of Lake  
476 Wakatipu. It is inferred that the delta foreset beds preserved on the eastern side  
477 of Mt Alfred, which outcrop there some 10 m above the modern Dart floodplain,  
478 predate The Hillocks. Otherwise The Hillocks would have been underwater,  
479 which is precluded by the observation that they were emplaced onto a braid plain

480 and deltaic forest beds. This requires that the level of Lake Wakatipu had  
481 already dropped from its high-stand of approximately 360 m asl to lower than 340  
482 m asl by 7.9 ka as indicated by the elevation of the foreset beds underneath The  
483 Hillocks deposit (Figure 6), so that it was between 340 m asl and the present  
484 level of 309 m asl. This is consistent with Bell (1992) whose dating suggests a  
485 lake level of 335 m asl (26 m above present level) by ~ 10 ka. The Dart River  
486 delta (i.e. lake shoreline) therefore must also have been some distance  
487 downstream by this time; the modern delta is ~8 km from the downstream edge  
488 of The Hillocks. This provides a constraint on the maximum delta progradation  
489 rates, of 1 km ka<sup>-1</sup> (1 m a<sup>-1</sup>) on average since ~ 8 ka. Historical rates of  
490 progradation of the Rees-Dart delta, assessed from historical aerial photo  
491 interpretation by Wild (2013), are 1.7 m a<sup>-1</sup> from 1966 to 2007 (averaged from an  
492 aerial increase of 203,000 m<sup>2</sup> over a delta width of 2850 m). Likewise, modelled  
493 average progradation over the next 120 years is 1.4 m a<sup>-1</sup>, with a range of  
494 between 0.4 and 2.5 m a<sup>-1</sup> (Wild, 2013). These historical and projected rates are  
495 higher than the maximum rate estimated since 8 ka. This discrepancy suggests  
496 that either by 8 ka the delta shoreline was relatively close to The Hillocks, and/or  
497 that historical sediment supply is higher than during the Holocene (possibly  
498 increasing once Rees River coalesced with Dart River) or geometrical changes  
499 (e.g. lake depth) have resulted in faster progradation.

500 We observed up to 4 m of fluvial sediments draped between the hummocky  
501 topography of The Hillocks, so the Dart River has occupied a surface (5-6 m)  
502 higher than its modern channel since the emplacement of The Hillocks. The



503 topographic profiling (Figure 7 D) and the pattern of braid plain channels (Figure  
504 2) suggest paleo channels flowed towards the south-west across The Hillocks  
505 from the north-eastern edge of the deposit (an area of low, small mounds).  
506 Subsequent headward incision between, or connection through, some of the  
507 larger mounds on the west may have eventually allowed a channel avulsion to  
508 produce the present configuration, which appears today to be stable, and with  
509 The Hillocks constricting the river at this point. The elevated alluvial surface may  
510 relate to aggradation associated with delta progradation and its abandonment  
511 may relate to continued lowering of the level of Lake Wakatipu. Wild (2013)  
512 noted that aggradation-degradation phases may be a characteristic of the Dart  
513 River floodplain, and this may also explain our observation of terraces (i.e.  
514 incision) at the base of the rock avalanche (Figure 6 C). Alternatively, the surface  
515 and its abandonment may relate to a blockage of the Dart River by the rock  
516 avalanche, possibly driving temporary ponding and aggradation upstream,  
517 overtopping, and eventual breaching following channel avulsion through the  
518 larger mounds to the west.

519 McColl and Davies (2011) suggested that The Hillocks may be a coseismic  
520 landslide deposit based on the observation of a deep-seated source area at the  
521 top of a steep slope, consistent with observations made following other coseismic  
522 landslide events (McSaveney et al., 2000); by contrast, historical aseismic events  
523 in New Zealand more often involve the failure of a spur or slab of rock (e.g.  
524 Owens, 1992; Hancox et al., 2005). If a seismic event did trigger The Hillocks  
525 landslide at ~8 ka, it may have triggered other landslides in the region. Sweeney

526 et al. (2013) dated the Lochnagar landslide deposit, ~30 km northeast from The  
527 Hillocks, to between  $6.3 \pm 0.3$  to  $8.9 \pm 0.5$  ka, favouring an older age within this  
528 bracket. The authors did not specify a triggering mechanism, but suggested a  
529 seismic event could have initiated the failure. Thus, in addition to future work on  
530 dating glacial landforms, it would be valuable to date other pre-historic landslide  
531 deposits in the region (e.g. those farther up the Dart River; Cox et al., 2014) in  
532 order to determine whether there is a broader evidence base for a major  
533 earthquake at this time.

534

## 535 **Conclusions**

536 Information on landform morphometry, sedimentology, and age presented in  
537 this study favour a rock avalanche origin for The Hillocks in Otago, New Zealand.  
538 Clast morphologies within The Hillocks deposit are consistent with rock  
539 avalanche deposits, but not with other proposed deposits or mechanisms. The  
540 morphology and distribution of the mounds suggests thinning of the deposit, and  
541 reduction in mound size in a cross-valley direction away from the proposed  
542 source area. The most plausible source area identified for the landslide seems to  
543 be the basin to the west, which has a scar with a volume compatible with the  
544 volume measured for The Hillocks, and has produced boulders with a lithology  
545 matching that of The Hillocks. GPR data indicate that the deposit was emplaced  
546 upon a braid plain and prograded delta.  $^{10}\text{Be}$  exposure-ages of ~ 7.9 ka for the  
547 mounds, and statistically-indistinguishable ages for adjacent landforms assumed

548 to be related, provide further support for a rock avalanche origin, and indicate a  
549 Holocene timing for that event. These new data show that by 7.9 ka the former  
550 Wakatipu Glacier had certainly retreated up valley past this location, and Dart  
551 River had prograded down valley of this location, providing useful constraints on  
552 glacial and post-glacial chronologies in the otherwise fragmentary record of  
553 events in this catchment. Furthermore, this study demonstrates the utility of  
554 quantitative methods of landform identification and analysis for informing studies  
555 that utilise landforms for paleoclimate or landscape reconstructions.

556

## 557 **Acknowledgements**

558 We thank Duncan Quincey, Emma Cody, and Florian Strohmaier for  
559 assistance in the field; Otago Regional Council for supplying LiDAR data; Sacha  
560 Baldwin and Gregory De Pascal for assistance with cosmogenic sample  
561 preparation; and the land custodians for access to the field site. SJC  
562 acknowledges funding from the Aberystwyth University Research Fund, STM  
563 acknowledges funding from Massey University (RM17927). Much of the analysis  
564 and writing of this manuscript was undertaken whilst SJC was in receipt of a  
565 Massey University Visiting Scholarship and STM in receipt of a University of  
566 Dundee ISSR Global Scholar grant. We are grateful to the three reviewers who  
567 provided thoughtful suggestions which helped us to improve this manuscript.

568

## 569 **References**

- 570 Alexander, D., Davies, T., Shulmeister, J., 2014. Formation of the Waiho Loop  
571 terminal moraine, New Zealand. *Journal of Quaternary Science*, 29(4), 361-  
572 369.
- 573 Alloway, B.V., Lowe, D.J., Barrell, D.J., et al., 2007. Towards a climate event  
574 stratigraphy for New Zealand over the past 30 000 years (NZ-INTIMATE  
575 project). *Journal of Quaternary Science*, 22(1), 9-35.
- 576 Balco, G., Stone, J.O., Lifton, N.A., et al., 2008. A complete and easily accessible  
577 means of calculating surface exposure ages or erosion rates from  $^{10}\text{Be}$  and  
578  $^{26}\text{Al}$  measurements. *Quaternary Geochronology*, 3(3), 174-195.
- 579 Ballantyne, C.K., 2018. Glacially moulded landslide runout debris in the Scottish  
580 Highlands. *Scottish Geographical Journal*, 134(3-4), 224-236.
- 581 Barrell, D.J.A., 2011. Quaternary glaciers of New Zealand. In: J. Ehlers, P.L.  
582 Gibbard, P.D. Hughes (Eds.), *Developments in Quaternary Science*, 15,  
583 1047-1064. Elsevier.
- 584 Barrell, D.J.A. 2019. General distribution and characteristics of active faults and  
585 folds in the Queenstown Lakes and Central Otago districts, Otago. Lower  
586 Hutt (NZ): GNS Science. Consultancy Report 2018/207.
- 587 Bell, D.H., 1992. Geomorphic evolution of a valley system: The Kawarau Valley,  
588 Central Otago. In: J.M. Soons, M.J. Selby (Eds.), *Landforms of New Zealand*.  
589 Longman, Auckland, pp. 456-481.
- 590 Benn, D.I., Ballantyne, C.K., 1994. Reconstructing the transport history of  
591 glacial sediments: a new approach based on the co-variance of clast form  
592 indices. *Sedimentary Geology*, 91(1-4), 215-227.
- 593 Benn, D.I., 2004. Clast morphology. In: Evans, D.J.A., Benn, D.I. (Eds.), *A  
594 Practical Guide to the Study of Glacial Sediments*. Arnold, London.

- 595 Brodie, J.W., Irwin, J., 1970. Morphology and sedimentation in Lake Wakatipu,  
596 New Zealand. *New Zealand Journal of Marine & Freshwater Research*, 4(4),  
597 479-496.
- 598 Brook, M., Lukas, S., 2012. A revised approach to discriminating sediment  
599 transport histories in glacial sediments in a temperate alpine  
600 environment: a case study from Fox Glacier, New Zealand. *Earth Surface  
601 Processes and Landforms*, 37(8), 895-900.
- 602 Cook, S.J., Porter, P.R., Bendall, C.A., 2013. Geomorphological consequences  
603 of a glacier advance across a paraglacial rock avalanche deposit.  
604 *Geomorphology*, 189, 109-120.
- 605 Cook, S.J., Quincey, D.J., Brasington, J., 2014. Geomorphology of the Rees  
606 Valley, Otago, New Zealand. *Journal of Maps*, 10(1), 136-150.
- 607 Corominas, J., 1996. The angle of reach as a mobility index for small and large  
608 landslides. *Canadian Geotechnical Journal*, 33(2), 260-271.
- 609 Cox, S.C., Rattenbury, M.S., McSaveney, et al., 2014. Activity of the Landslide  
610 Te Horo and Te Koroka Fan, Dart River, New Zealand During January 2014.  
611 GNS Science Report 2014/07, 45 pp.
- 612 Denton, G.H., Heusser, C., Lowell, T., et al., 1999. Interhemispheric linkage of  
613 paleoclimate during the last glaciation. *Geografiska Annaler: Series A,  
614 Physical Geography*, 81(2), 107-153.
- 615 Dufresne, A., 2009. Influence of runout path material on rock and debris  
616 avalanche mobility: field evidence and analogue modelling. Doctor of  
617 Philosophy PhD Thesis, University of Canterbury, Christchurch, 268 pp.
- 618 Dufresne, A., Davies, T.R., 2009. Longitudinal ridges in mass movement  
619 deposits. *Geomorphology* 105(3-4), 171–181.

- 620 Dufresne, A., Bösmeier, A., Prager, C., 2016. Sedimentology of rock avalanche  
621 deposits—case study and review. *Earth-Science Reviews*, 163, 234-259.
- 622 Dunning, S., 2006. The grain size distribution of rock-avalanche deposits in  
623 valley-confined settings. *Italian Journal of Engineering Geology and*  
624 *Environment*, 1, 117-121.
- 625 Goudie, A.S., 2006. The Schmidt Hammer in geomorphological research.  
626 *Progress in Physical Geography*, 30(6), 703-718.
- 627 Hancox, G.T., McSaveney, M.J., Manville, V.R., et al., 2005. The October 1999  
628 Mt Adams rock avalanche and subsequent landslide dam-break flood and  
629 effects in Poerua River, Westland, New Zealand. *New Zealand Journal of*  
630 *Geology and Geophysics*, 48(4), 683-705.
- 631 Hewitt, K., 1999. Quaternary moraines vs catastrophic rock avalanches in the  
632 Karakoram Himalaya, Northern Pakistan. *Quaternary Research*, 51(3), 220-  
633 237.
- 634 Hewitt, K., 2009. Catastrophic rock slope failures and late Quaternary  
635 developments in the Nanga Parbat-Haramosh Massif, Upper Indus basin,  
636 northern Pakistan. *Quaternary Science Reviews*, 28(11-12), 1055-1069.
- 637 Jones, R.S., Small, D., Cahill, N., et al., 2019. iceTEA: Tools for plotting and  
638 analysing cosmogenic-nuclide surface-exposure data from former ice  
639 margins. *Quaternary Geochronology*, 51, 72-86.
- 640 Kaplan, M.R., Schaefer, J.M., Denton, G.H., et al., 2013. The anatomy of long-  
641 term warming since 15 ka in New Zealand based on net glacier snowline  
642 rise. *Geology*, 41(8), 887-890.
- 643 Kenny, J.A., Hayward, B.W., 1993. Inventory of Important Geological Sites and  
644 Landforms in the Otago Region. Geological Society of New Zealand  
645 Miscellaneous Publication, 77.

- 646 Kober, F., 1999. Late Quaternary Geology of Glenorchy District, Upper Lake  
647 Wakatipu. Postgraduate Diploma of Science of Geology Thesis, University of  
648 Otago, Dunedin, 121 pp.
- 649 Lukas, S., Benn, D.I., Boston, C.M., et al., 2013. Clast shape analysis and clast  
650 transport paths in glacial environments: A critical review of methods and the  
651 role of lithology. *Earth-Science Reviews*, 121, 96-116.
- 652 McColl, S.T., Davies, T.R., 2011. Evidence for a rock-avalanche origin for 'The  
653 Hillocks' "moraine", Otago, New Zealand. *Geomorphology*, 127(3-4), 216-  
654 224.
- 655 McSaveney, M.J., Davies, T.R., Hodgson, K.A., 2000. A contrast in deposit style  
656 and process between large and small rock avalanches. In: E. Bromhead, N.  
657 Dixon, M.L. Ibsen (Eds.), VIII ISL Cardiff, Landslides in research, theory and  
658 practice. *Landslides*. Thomas Telford, London, 1053-1058 pp.
- 659 Ostermann, M., Sanders, D., Ivy-Ochs, S., et. al., 2012. Early Holocene (8.6 ka)  
660 rock avalanche deposits, Obernberg valley (Eastern Alps): Landform  
661 interpretation and kinematics of rapid mass movement. *Geomorphology*, 171,  
662 83-93.
- 663 Owens, I.F., 1992. A note on the Mount Cook Rock Avalanche of 14 December  
664 1991. *New Zealand Geographer*, 48(2), 74-78.
- 665 Paguican, E., de Vries, B.v.W., Lagmay, A., 2014. Hummocks: how they form  
666 and how they evolve in rockslide-debris avalanches. *Landslides*, 11(1), 67-  
667 80.
- 668 Powers, M.C., 1953. A new roundness scale for sedimentary particles. *Journal of*  
669 *Sedimentary Research*, 23(2), 117-119.

- 670 Putnam, A.E., Schaefer, J.M., Barrell, D.J.A., et al., 2010a. In situ cosmogenic  
671  $^{10}\text{Be}$  production-rate calibration from the Southern Alps, New Zealand.  
672 *Quaternary Geochronology*, 5(4), 392-409.
- 673 Putnam, A.E., Denton, G.H., Schaefer, et al., 2010b. Glacier advance in southern  
674 middle-latitudes during the Antarctic Cold Reversal. *Nature Geoscience*,  
675 3(10), 700-704.
- 676 Reznichenko, N.V., Davies, T.R., Winkler, S., 2016. Revised palaeoclimatic  
677 significance of Mueller Glacier moraines, Southern Alps, New Zealand. *Earth*  
678 *Surface Processes and Landforms*, 41(2), 196-207.
- 679 Schaefer, J.M., Denton, G.H., Barrell, D.J.A., et al., 2006. Near-synchronous  
680 interhemispheric termination of the Last Glacial Maximum in mid-latitudes.  
681 *Science*, 312(5779), 1510-1513.
- 682 Schaefer, J.M., Denton, G.H., Kaplan, M., et al., 2009. High-Frequency Holocene  
683 Glacier Fluctuations in New Zealand Differ from the Northern Signature.  
684 *Science*, 324(5927), 622-625.
- 685 Schleier, M., Hermanns, R.L., Rohn, J. e.t. al., 2015. Diagnostic characteristics  
686 and paleodynamics of supraglacial rock avalanches, Innerdalen, Western  
687 Norway. *Geomorphology*, 245, 23-39.
- 688 Stirling, M., McVerry, G., Gerstenberger, M., et al., 2012. National seismic hazard  
689 model for New Zealand: 2010 update. *Bulletin of the Seismological Society of*  
690 *America*, 102(4), 1514-1542.
- 691 Sutherland, R., Kim, K., Zondervan, A., et al., 2007. Orbital forcing of mid-latitude  
692 Southern Hemisphere glaciation since 100 ka inferred from cosmogenic  
693 nuclide ages of moraine boulders from the Cascade Plateau, southwest New  
694 Zealand. *Geological Society of America Bulletin*, 119(3-4), 443-451.



- 695 Sutherland, J.L., Carrivick, J.L., Shulmeister, J., et al., 2019. Ice-contact  
696 proglacial lakes associated with the Last Glacial Maximum across the  
697 Southern Alps, New Zealand. *Quaternary Science Reviews*, 213, 67-92.
- 698 Sweeney, C.G., Brideau, M.A., Augustinus, P.C., et al., 2013. Lochnagar  
699 landslide-dam – Central Otago, New Zealand: Geomechanics and timing of  
700 the event, In C.Y Chin (Ed.), 19th New Zealand Geotechnical Society 2013  
701 Symposium: Hanging by a thread?: lifelines, infrastructure and natural  
702 disasters, Queenstown, November 2013. Wellington, NZ: Institute of  
703 Professional Engineers New Zealand. Proceedings of technical groups  
704 (Institution of Professional Engineers New Zealand).
- 705 Thomson, R., 1996. Prehistoric changes in the level of Lake Wakatipu. An  
706 unpublished outline study prepared for the Otago Regional Council, 4 pp.
- 707 Turnbull, I.M., 2000 (compiler). Geology of the Wakatipu area, Institute of  
708 Geological and Nuclear Sciences 1:250 000 geological map 18. Institute of  
709 Geological and Nuclear Sciences Limited, Lower Hutt, New Zealand. Map (1  
710 sheet) + 72 pp.
- 711 Wild, M.A., 2013. Growth dynamics of braided gravel-bed river deltas in New  
712 Zealand. PhD Thesis, University of Canterbury, Christchurch, 246 pp.
- 713 Winkler, S., 2014. Investigation of late-Holocene moraines in the western  
714 Southern Alps, New Zealand, applying Schmidt-hammer exposure-age  
715 dating. *The Holocene*, 24(1), 48-66.
- 716 Wood, J.R., Wilmshurst, J.M. & Rawlence, N.J. 2011. Radiocarbon-dated faunal  
717 remains correlate very large rock avalanche deposit with prehistoric Alpine  
718 fault rupture. *New Zealand Journal of Geology and Geophysics*, 54, 431-434.
- 719

720

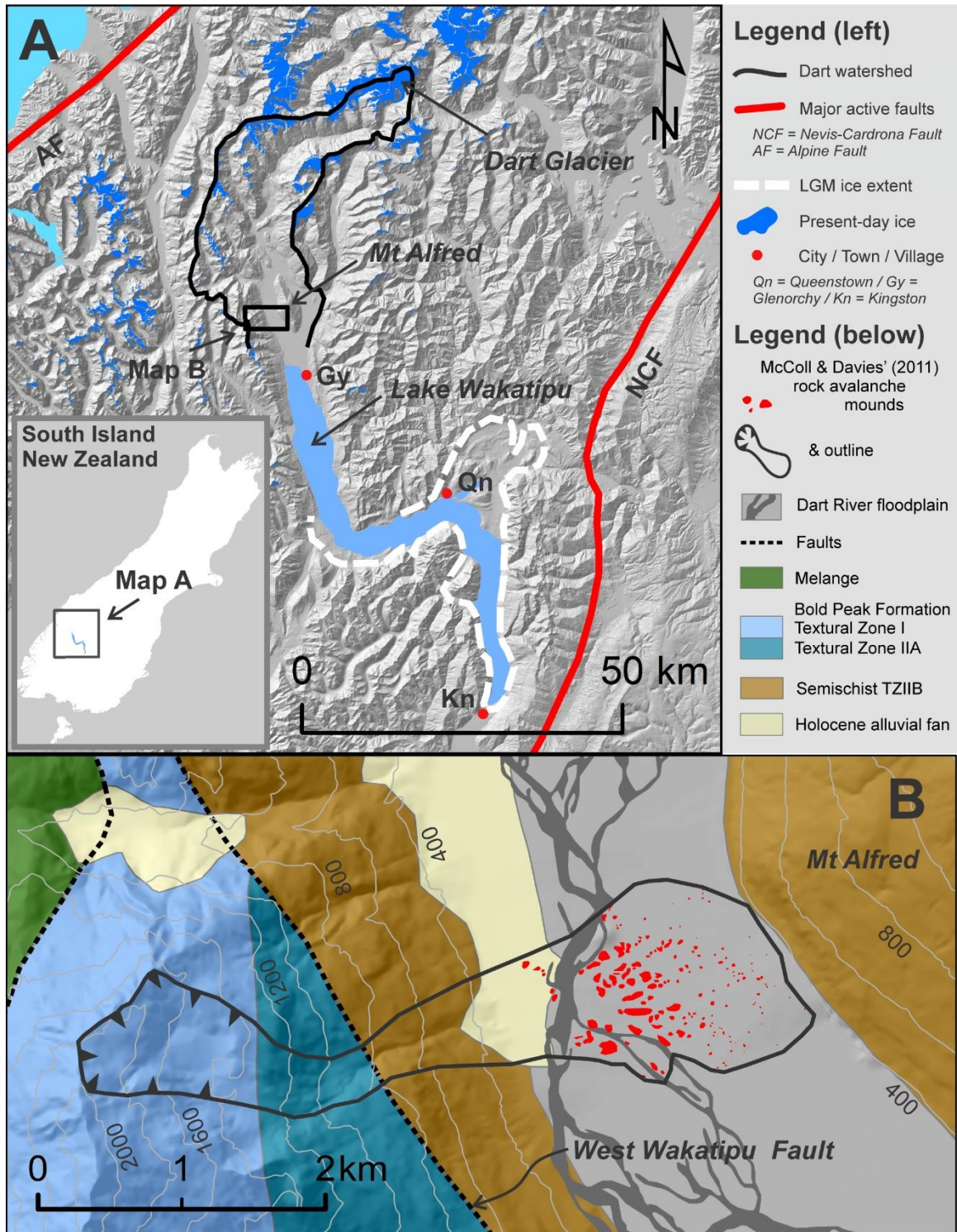
**Table 1:** Cosmogenic  $^{10}\text{Be}$  exposure age measurements and parameters.

Sample name	Feature / location	Latitude	Longitude	Elevation (m asl)	Thickness (cm)	Density ( $\text{g cm}^{-3}$ )	Shielding correction	Be-10 atoms $\text{g}^{-1}$	Be AMS standard	Age $\pm 1 \sigma$ (ka) (external error in brackets)
WP166	Near source	-44.78	168.30	1400	1.5	2.7	0.871	$87194 \pm 3337$	NIST_27900	$7.55 \pm 0.29$ (0.31)
HB20	Mound	-44.77	168.33	352	1.5	2.7	0.988	$40031 \pm 2600$	NIST_27900	$7.55 \pm 0.49$ (0.51)
HB14	Mound	-44.77	168.33	345	1.5	2.7	0.987	$43977 \pm 2878$	07KNSTD	$8.32 \pm 0.55$ (0.56)
HB24	Debris fan	-44.77	168.32	350	1.5	2.7	0.975	$36649 \pm 2372$	07KNSTD	$7.04 \pm 0.46$ (0.47)

721

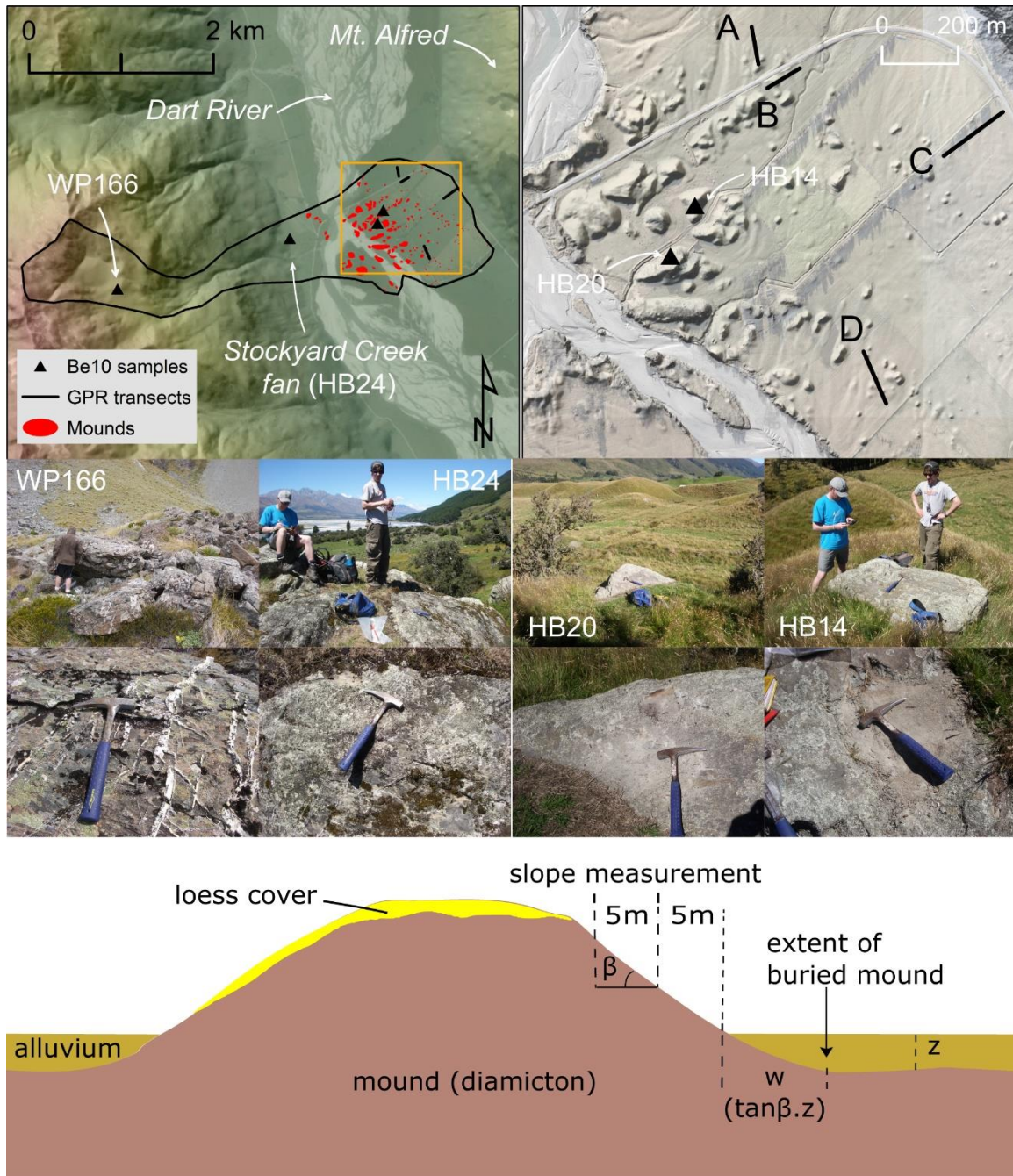
722

723 **Figures:**



727 the Dart River catchment, major active faults, modern and former ice extents and  
728 present-day Dart Glacier; see inset map for location within New Zealand's South  
729 Island. Map B) The Hillocks Rock Avalanche outline and distribution of mounds  
730 (according to McColl and Davies, 2011), with general topography and major rock  
731 types and faults shown (from Turnbull, 2000).

732



733

734 **Figure 2.** Maps showing the positioning of GPR transects and  $^{10}\text{Be}$   
735 cosmogenic exposure age dating sampling locations. Left-hand map shows  
736 outline of the rock avalanche (black outline) and mounds (red polygons) as  
737 mapped by McColl and Davies (2011). A transparent LINZ 8 m DEM hillshade  
738 behind an aerial image provides an impression of topographic relief. The right-

739 hand map shows the mounds on the floodplain, with a LiDAR hillshade model.  
740 The photos show the  $^{10}\text{Be}$  cosmogenic sample sites and sampled boulders. The  
741 conceptual diagram below demonstrates how the extents of partially buried  
742 mounds were approximated.

743

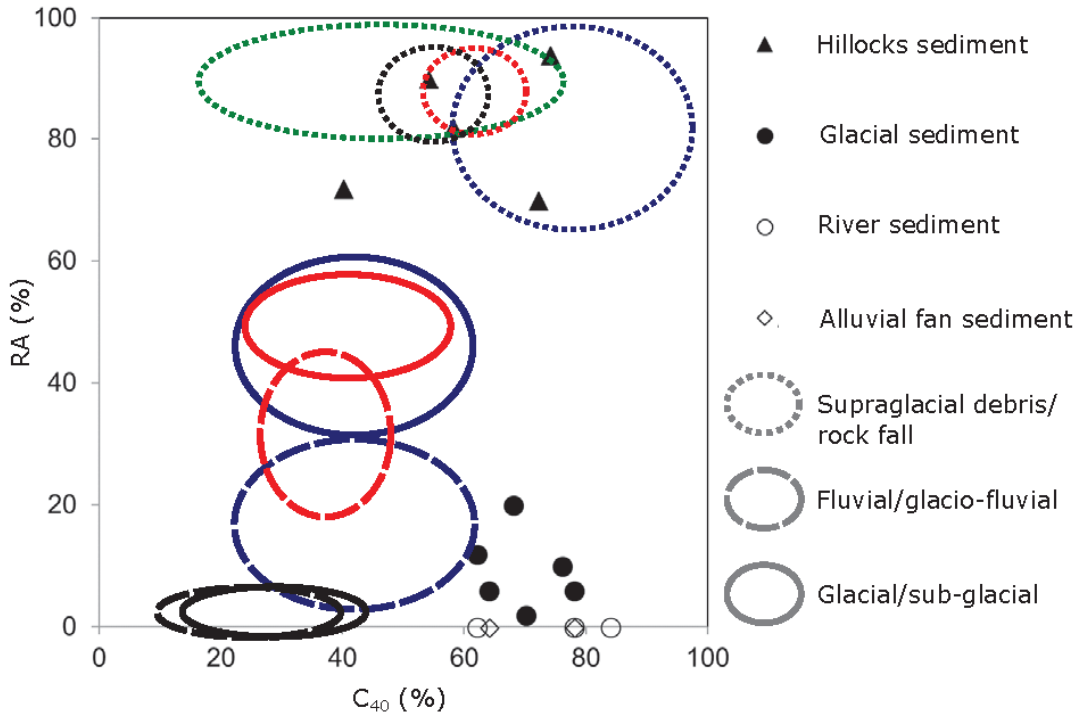


744

745 **Figure 3:** Sediments from exposures at The Hillocks: A) Streambank of the  
746 Stockyard Creek as it dissects the debris fan, with a notable lack of bedding,  
747 suggesting rapid emplacement possibly by the rock avalanche; B) Close up of  
748 rock avalanche sediments showing angular nature; C) Exposure of rock  
749 avalanche sediments with large boulder on top; boulder-carapaces are common

750 in rock avalanche deposits; D) Exposure of a mound at the Dart River with rock  
751 avalanche sediments on right (near person's legs) and coarse fluvial gravels on  
752 left, with fines (loess and / overbank silts) on top.

753



754

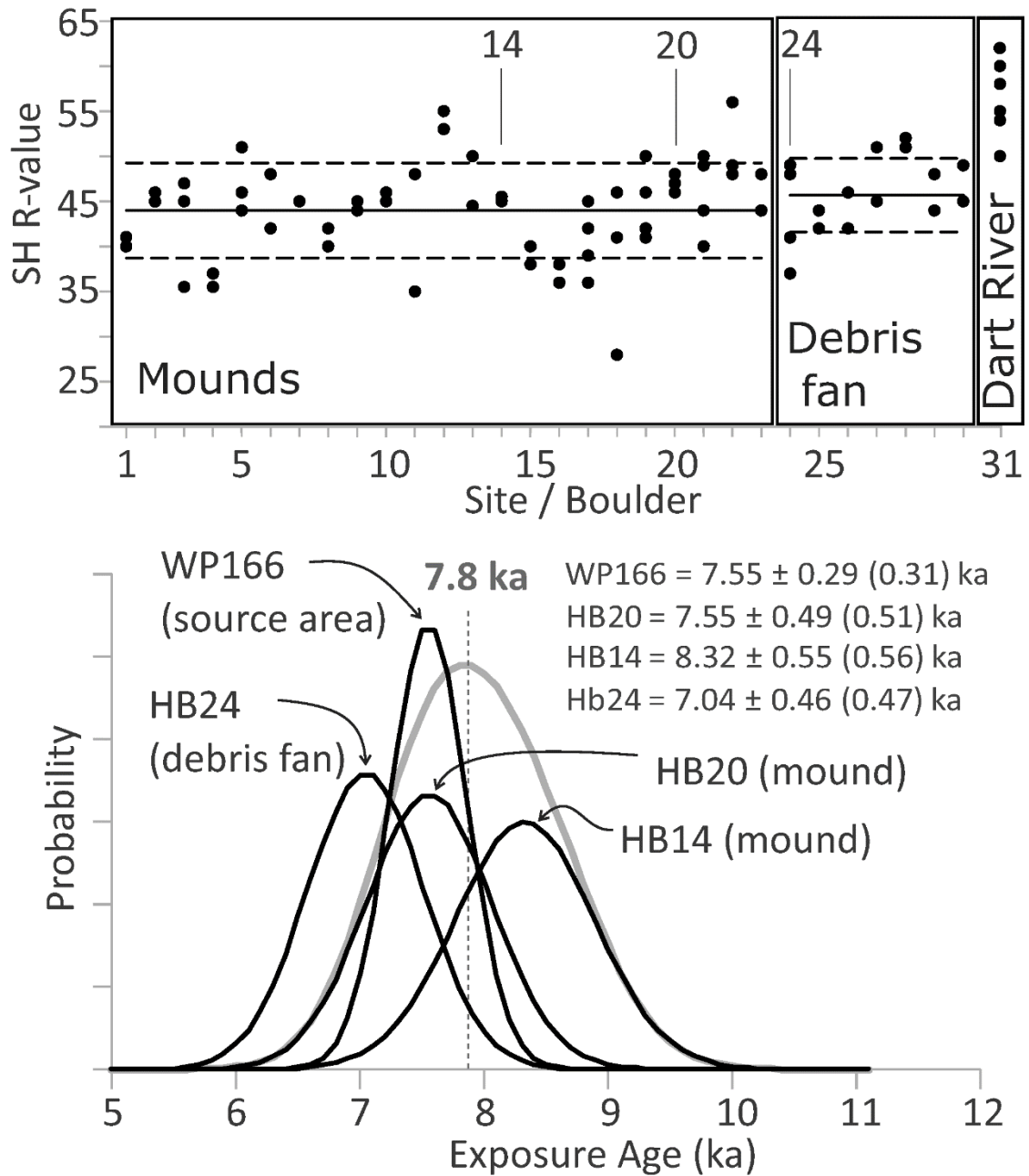
755 **Figure 4:** C<sub>40</sub>-RA plot of clast data collected from The Hillocks and a range of  
756 other comparison sediment types. The RA axis represents the percentage of  
757 clasts that are angular and very angular; the C<sub>40</sub> axis represents the proportion of  
758 clasts with a c:a axial ratio of  $\leq 0.4$  (i.e. more slabby and elongate shapes). The  
759 ellipses represent envelopes for characteristic sediment types; blue envelopes  
760 from Lukas et al. (2013) for high-mountain glaciers worldwide; red and black  
761 envelopes from Brook and Lukas (2012) for Fox Glacier, New Zealand, for schist

762 and greywacke respectively; green envelope from Reznichenko et al. (2016) for a  
763 rock-avalanche dominated moraine at Mueller Moraine, New Zealand.

764

765





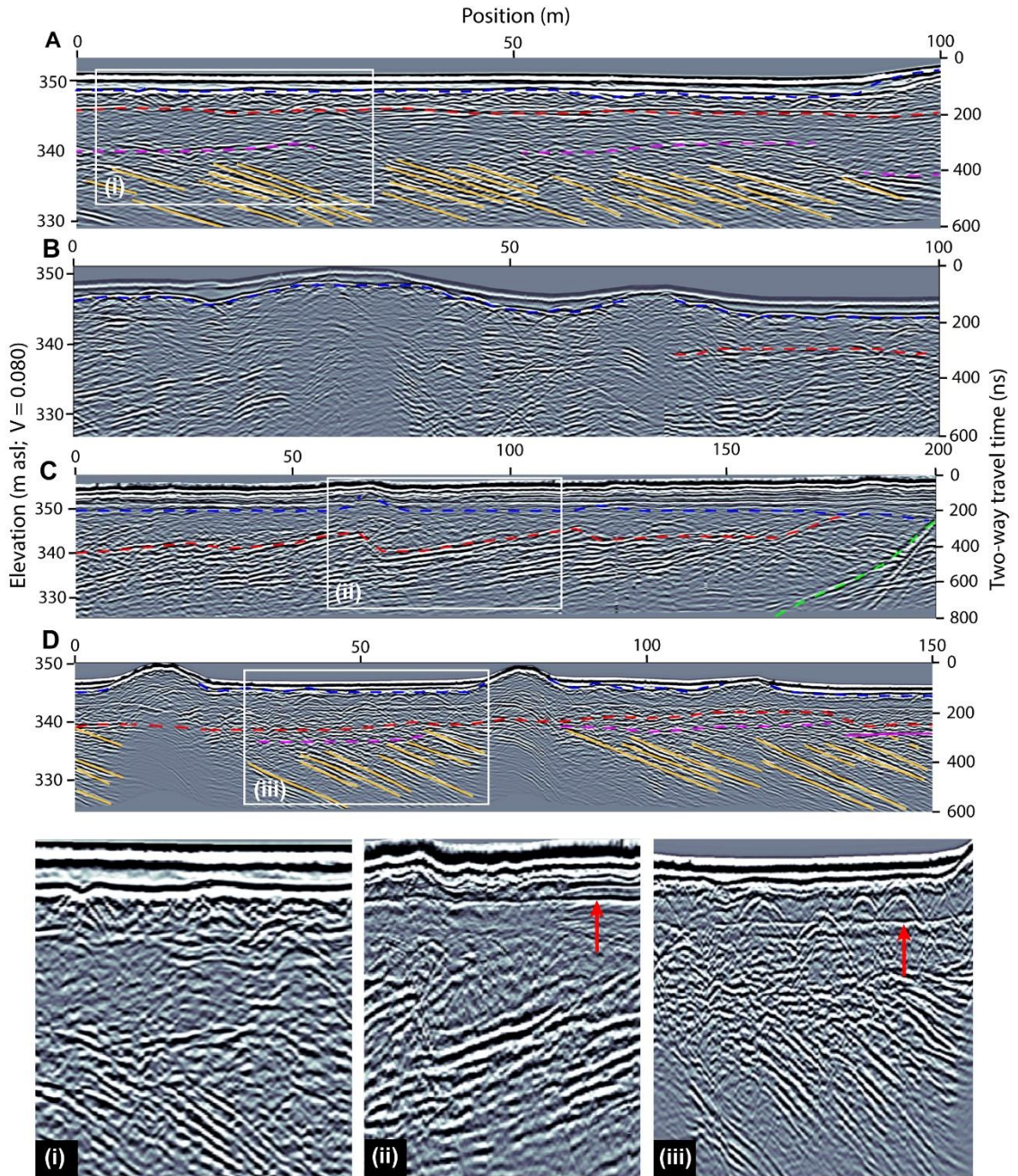
766

767 **Figure 5.** Top) Schmidt hammer rebound values for boulders on the  
768 floodplain mounds, debris fan, and within the Dart River channel. Dots represent  
769 single R-values. Boxes distinguish different sampling location. The Dart River  
770 (31) represents aggregated values for several boulders within the channel,

771 whereas the floodplain and debris fan sites (i.e. boulders 1-30) have values  
772 shown for individual boulders. Solid lines show the mean value and dashed lines  
773 are  $\pm 1 \sigma$ , for the floodplain and debris fan separately. Arrows indicate boulders  
774 used for cosmogenic sampling. Bottom)  $^{10}\text{Be}$  exposure ages and their probability  
775 density functions. Individual ages (black) are plotted as probability density  
776 functions (PDF) of a normal distribution using the measured exposure age and  
777 the ( $1 \sigma$ ) external (i.e. measurement + production rate) uncertainty. The grey line  
778 shows the sum of the individual PDFs for the two mound samples. The peak of  
779 the summed PDF plot (solid line) presents a clustered age of 7.8 ka.

780

781

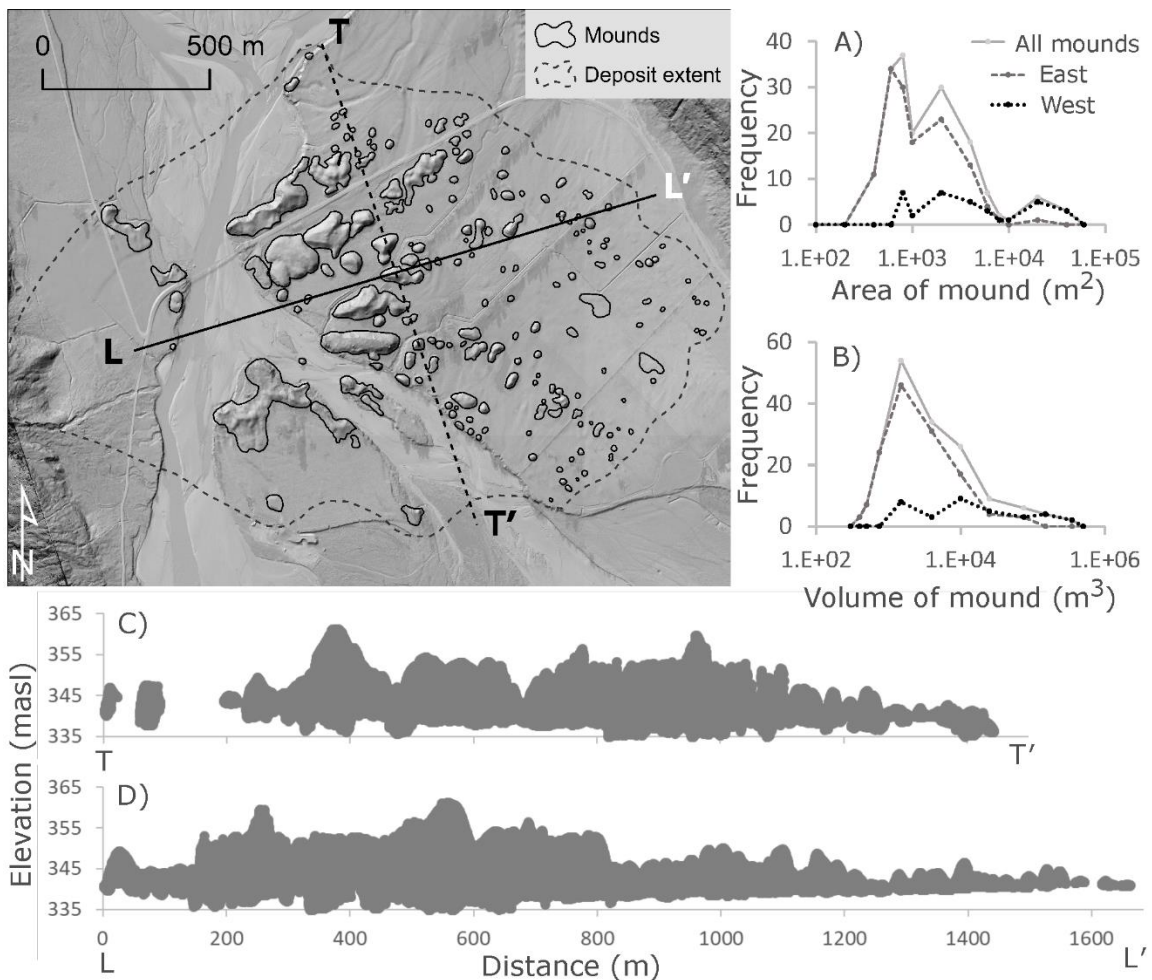


782

783 **Figure 6:** Radargrams from Transects A-D, with zoomed sections shown in  
784 panels i-iii. The locations are found in Figure 2, with the beginning position (left-  
785 hand side) of each transect shown by the position of the letter labels in Figure 2.  
786 Representative annotations are as follows: Blue dashed line = base of alluvial fill;

787 Red dashed line = base of chaotic/diamicton-like material; Orange line = foreset  
788 beds; Purple dashed line = angular contact between foreset beds and overlaying  
789 alluvium; Green dashed line; top of colluvium/bedrock of Mt Alfred; Red arrows  
790 show reflector interpreted to be water table. The zoomed in panels i-iii have  
791 vertical exaggeration, whereas panels A-D have approximately equal distance-  
792 depth scales.

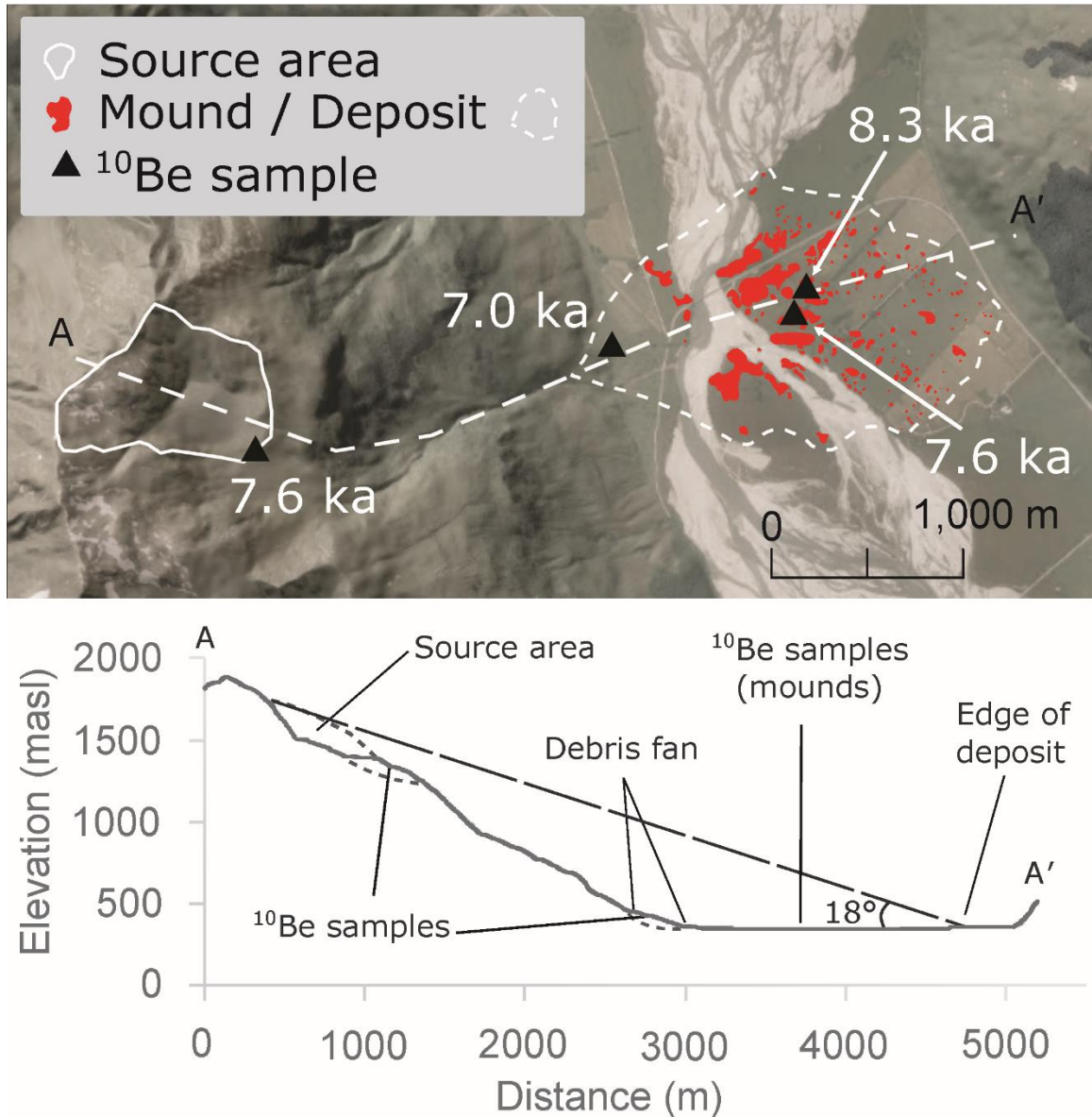
793



794

795        **Figure 7:** Area (A) and volume (B) frequency distribution curves are shown for  
796 all mounds (and also divided into mounds east and west of line T-T' on inset map).  
797 Point elevation swath plots of the mounds are shown in transverse (C) and  
798 longitudinal (D) directions relative to hypothesised avalanche travel direction; inset  
799 map shows centreline of the transverse (T-T') and longitudinal (L-L') swaths, and  
800 the distribution of mounds updated in this study.

801



802

803 **Figure 8:** Map showing rock avalanche source area and deposit as mapped  
804 in this study, with  $^{10}\text{Be}$  exposure ages. Cross-section below is extracted from  
805 LINZ 8 m DEM for the transect A-A' shown on the map; the dashed lines  
806 represent possible pre-failure topography. The travel angle of  $\tan^{-1}(H/L) = 18^\circ$  is  
807 slightly higher than (the  $14^\circ$ ) estimated using Coriminas' (1996) empirical  
808 regression model, for a rockfall/avalanche volume of  $22.5 \text{ M m}^3$ , but it is within  
809 the normal range for rock avalanches.